Molecular Microbiology (2014) 93(6), 1172–1182 ■
doi:10.1111/mmi.12726
First published online 11 August 2014

A transcription factor links growth rate and metabolism in the hypersaline adapted archaeon *Halobacterium salinarum*

Horia Todor,[1] Keely Dulmage,[1,2†] Nicholas Gillum,[1†] James R. Bain,[3] Michael J. Muehlbauer[3] and Amy K. Schmid[1,2,4*]

[1]*Department of Biology,* [2]*University Program in Genetics and Genomics, and* [4]*Center for Systems Biology, Duke University, Durham, NC 27708, USA.*

[3]*Sarah W. Stedman Nutrition and Metabolism Center, Duke Molecular Physiology Institute, Durham, NC 27710, USA.*

Summary

Co-ordinating metabolism and growth is a key challenge for all organisms. Despite fluctuating environments, cells must produce the same metabolic outputs to thrive. The mechanisms underlying this 'growth homeostasis' are known in bacteria and eukaryotes, but remain unexplored in archaea. In the model archaeon *Halobacterium salinarum*, the transcription factor TrmB regulates enzyme-coding genes in diverse metabolic pathways in response to glucose. However, *H. salinarum* is thought not to catabolize glucose. To resolve this discrepancy, we demonstrate that TrmB regulates the gluconeogenic production of sugars incorporated into the cell surface S-layer glycoprotein. Additionally, we show that TrmB–DNA binding correlates with instantaneous growth rate, likely because S-layer glycosylation is proportional to growth. This suggests that TrmB transduces a growth rate signal to co-regulated metabolic pathways including amino acid, purine, and cobalamin biosynthesis. Remarkably, the topology and function of this growth homeostatic network appear conserved across domains despite extensive alterations in protein components.

Introduction

The co-ordination of growth with catabolic and anabolic metabolism is one of the most important and complicated tasks an organism faces (Brauer *et al.*, 2008). Cells must regulate diverse processes in response to environmental conditions and nutrient availability so that the appropriate metabolic outputs are produced in the correct proportions for the cell to continue to grow, replicate, and maintain energetic balance. This balance, here referred to as growth homeostasis, must also be co-ordinated with cell cycle, shape, and division (Johnston *et al.*, 1977). Because of its importance to all organisms, various aspects of growth homeostasis have been elucidated for several organisms in the bacterial and eukaryotic domains (Weart *et al.*, 2007; Brauer *et al.*, 2008). Despite the importance of growth homeostasis, the connection between cell growth and metabolism remains understudied in the archaea. Elucidation of the mechanisms for co-ordinating growth rate and metabolism in this third domain of life is necessary to provide a complete perspective on the evolution of growth homeostatic mechanisms in different environmental niches.

In previous work, we identified and characterized a transcription factor, TrmB, in the hypersaline archaeon *Halobacterium salinarum*. TrmB regulates genes coding for enzymes involved in diverse metabolic pathways in response to glucose (Schmid *et al.*, 2009). TrmB is a helix–turn–helix transcription factor whose amino acid sequence and *cis*-regulatory DNA-binding motif are strongly conserved throughout the archaeal domain (Lee *et al.*, 2003; 2007; Schmid *et al.*, 2009; Perez-Rueda and Janga, 2010). This transcription factor has been shown to be involved in the regulation of maltose, trehalose, and glucose uptake and metabolism throughout the archaeal domain (Kanai *et al.*, 2007; Lee *et al.*, 2008; Schmid *et al.*, 2009). In *H. salinarum*, TrmB binds to the promoters of over 100 genes that encode enzymes functioning throughout central and peripheral metabolism during growth on amino acids as the sole source of carbon and energy (i.e. in the absence of any added sugars; Schmid *et al.*, 2009). While bound to the DNA, TrmB represses some promoters (e.g. glycolytic enzyme-coding genes) and activates others (e.g. gluconeogenic genes). TrmB–DNA binding is inhibited by a direct interaction with glucose in hyperthermophilic archaea (Krug *et al.*, 2006) and by glucose addition to the medium in *H. salinarum*. This leads to de-repression and de-activation of bound promoters. Through this mechanism, TrmB dynamically regulates the expression of enzyme-coding genes and transcription factors in

Accepted 21 July, 2014. *For correspondence. E-mail amy.schmid@duke.edu; Tel. (+1) 919 613 4464; Fax (+1) 919 660 7293. †These authors contributed equally to this work.

response to nutrient changes (Schmid *et al*., 2009; Todor *et al*., 2013).

Despite the importance of glucose in regulating central metabolism via TrmB in *H. salinarum*, previous studies suggest that *H. salinarum* may not be able to catabolize glucose. Both the gene and the enzyme activity for phosphofructokinase are undetectable in this organism (Sonawat *et al*., 1990; Ng *et al*., 2000). *H. salinarum* also cannot use glucose as the sole source of carbon and energy (Gochnauer and Kushner, 1969), and does not actively transport glucose from the media, although glucose can passively enter the cell (Severina *et al*., 1990). Previous label tracing NMR experiments have also failed to detect the conversion of ^{13}C-labelled glucose to pyruvate (Sonawat *et al*., 1990). This evidence raises the question of why *H. salinarum* regulates much of its metabolism in response to glucose. Here we address this question by testing the hypothesis that one possible function of glucose is to serve as a precursor molecule to the N- and O-linked glycans that decorate the cell surface glycoprotein.

In most known archaea, the cell envelope consists of a paracrystalline S-layer protein (Mescher *et al*., 1974). The S-layer is solely responsible for maintaining the characteristic rod shape of *H. salinarum* (Mescher and Strominger, 1976). It consists of a single protein that comprises approximately 50% of the protein and most of the non-lipid carbohydrate of the cell envelope (Mescher *et al*., 1974). The S-layer protein of *H. salinarum* contains two different types of N-linked glycans, including a repeating unit pentasaccharide (one site) and small sulphated oligosaccharides (10–15 sites), as well as a single O-linked disaccharide unit (10–15 sites at C-terminus; Wieland, 1988). These carbohydrate modifications are required for the stability and shape maintaining function of the S-layer in *H. salinarum* and related halophilic archaea (Mescher and Strominger, 1976). For example, strains deleted for genes encoding enzymes that attach the glycoprotein to the S-layer (Δ*algB*) exhibit rounded morphology and shed S-layer proteins into the medium (Abu-Qarn *et al*., 2007).

Here we present evidence that *H. salinarum* produces monosaccharides through gluconeogenesis that serve as precursors for the glycans that decorate the S-layer cell surface protein, enabling cells to maintain their characteristic rod shape during active growth. Additionally, we present metabolomics and gene expression data suggesting that TrmB is required for appropriate levels of these monosaccharides. TrmB activity is correlated with instantaneous growth rate across conditions and timescales, likely because growth requires additional S-layer and therefore additional glycans. We hypothesize that by sensing the concentration of a gluconeogenic metabolite, TrmB regulates genes encoding enzymes involved in diverse metabolic processes in response to cell growth rate.

Results

The ΔtrmB mutant is round in the absence of glucose

The Δ*trmB* deletion mutant has been shown to be defective in gene regulation and exhibits significantly impaired growth rate in batch culture using amino acids as a source of carbon, nitrogen, and energy. These phenotypes are complemented upon the addition of glucose to the medium (Schmid *et al*., 2009; Todor *et al*., 2013). In order to determine the physiological effects of misregulated gene expression caused by the Δ*trmB* mutation at a single cell level, we quantified the size and shape of *H. salinarum* cells in the Δ*trmB* mutant and its isogenic Δ*ura3* parent strain during mid-log phase growth ($OD_{600} \sim 0.5$) in complete medium (CM) via phase-contrast microscopy. We observed that the Δ*trmB* mutant strain was significantly rounder than the normally rod-shaped isogenic Δ*ura3* parent strain in the absence of glucose ($P < 2 \times 10^{-22}$, Fig. 1, see Supplementary Table S1 for *P*-values of all comparisons). This effect is unlikely to be caused by slow growth, since *H. salinarum* normally becomes more rod-shaped when growth is stopped (Herrmann and Soppa, 2002). As expected from batch culture growth rate and gene expression phenotypes, this morphological defect is significantly complemented by the addition of 5% glucose to the medium (Fig. 1). In order to test whether this shape defect may be caused by deficient S-layer glycosylation, we added the glycosylation inhibitor 2-deoxy-D-glucose (2DG; Esko and Bertozzi, 2009) to cultures of the Δ*trmB* mutant strain and the isogenic Δ*ura3* parent strain. The Δ*ura3* strain lost its rod shape and became significantly rounder in the presence of 2DG ($P < 1 \times 10^{-15}$, Fig. 1, Supplementary Table S1). Because both strains take on similar morphology in the presence of a glycosylation inhibitor, these results are consistent with the hypothesis that the lack of proper glycosylation can cause a shape defect such as that observed in the Δ*trmB* mutant strain.

Carbohydrate staining suggests that ΔtrmB morphological defects are associated with reduced S-layer glycosylation

In order to assess directly whether the morphological defect of the Δ*trmB* mutant strain is caused by a glycosylation defect, we assayed the carbohydrate to protein ratio of the S-layer glycoprotein from the Δ*trmB* mutant strain and its isogenic Δ*ura3* parent strain using Colloidal Coomassie Blue (CCB) and Periodic Acid Schiff (PAS) stains on SDS-PAGE. The carbohydrate to protein staining ratio is known to correlate with the amount of protein glycosylation (Gralnick *et al*., 1982). Because the S-layer represents a large fraction of total protein (~ 5%; Van *et al*., 2008) and migrates substantially slower than any

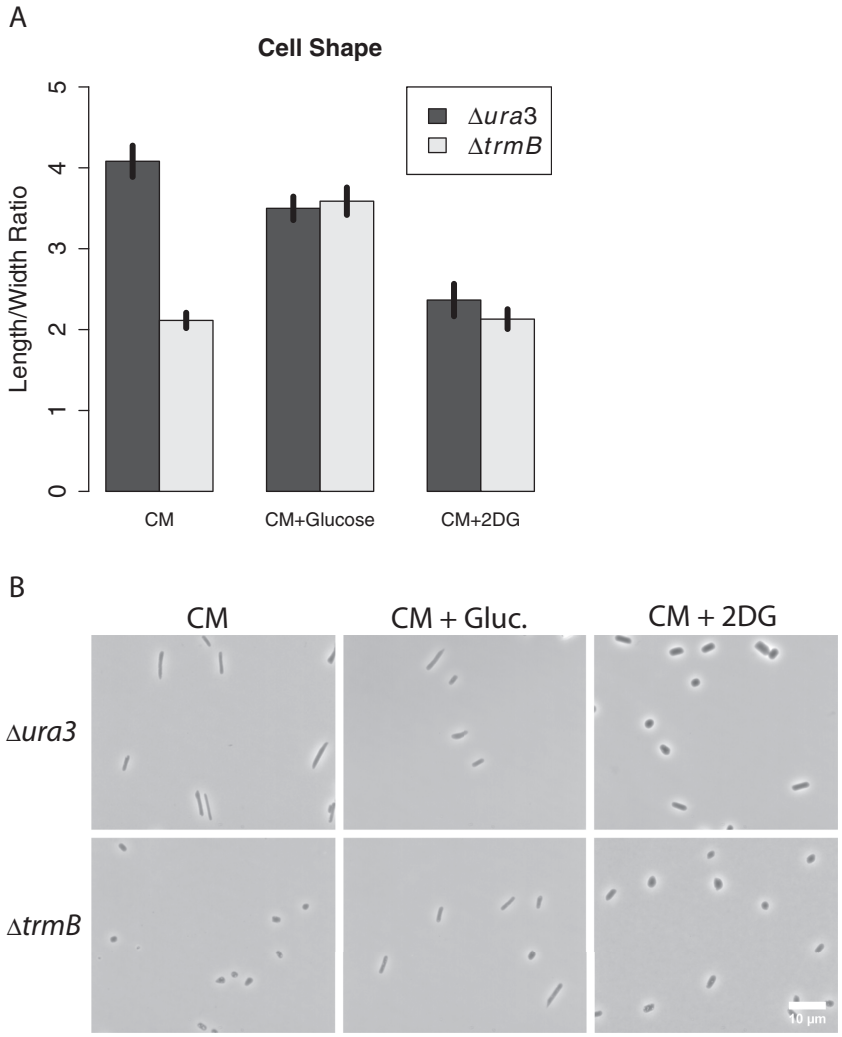

Fig. 1. The Δ*trmB* mutant strain exhibits altered cell morphology in the absence of glucose. Cells were visualized using phase-contrast microscopy and quantified by fitting an ellipse using ImageJ.
A. Bar graph shows the ratio of length to width in the Δ*ura3* parent strain (dark bars) and the Δ*trmB* mutant strain (light bars). Glucose complements the Δ*trmB* mutant's morphological phenotype, while the glycosylation inhibitor 2DG causes Δ*ura3* cells to assume the same morphology as the Δ*trmB* mutant strain. Error bars represent standard error of at least 39 measurements with an average of 114 cells.
B. Representative phase-contrast images of the Δ*ura3* parent strain and the Δ*trmB* mutant strain growing in CM, CM + 5% glucose, and CM + 2% 2DG.

other highly expressed protein (~ 200 kD), it is easily distinguishable from other proteins by SDS-PAGE. Whole cell lysates (*Experimental procedures*) from the Δ*trmB* mutant and its isogenic Δ*ura3* parent strain growing in either CM, CM supplemented with 5% glucose, or CM supplemented with 2% of the glycosylation inhibitor 2DG were compared. We observed that the Δ*trmB* mutant exhibited a significantly reduced carbohydrate to protein ratio in the S-layer protein compared to the Δ*ura3* parent strain in the absence of glucose (Fig. 2, $P < 2 \times 10^{-5}$, see Supplementary Table S2 for *P*-values of comparisons). The Δ*trmB* mutant strain also showed decreased carbohydrate staining of other proteins (Fig. 2B). Glucose increased the carbohydrate to protein ratio of S-layer glycoprotein from Δ*trmB* mutant cells to the level of the Δ*ura3* parent strain (see Supplementary Table S2 for *P*-values). In contrast, glucose did not substantially change the ratio in the Δ*ura3* parent strain. Consistent with its role as a glycosylation inhibitor and with the morphological data (Fig. 1), 2DG significantly reduced the carbohydrate to protein ratio in the Δ*ura3* strain (Fig. 2; $P < 0.002$), and only slightly further reduced this ratio in the Δ*trmB* mutant strain. These trends are recapitulated in S-layer enriched preparations (Supplementary Fig. S1). 2DG also increased electrophoretic mobility of the S-layer protein in both strains, consistent with S-layer lacking glycosyl modifications (Fig. 2B). Taken together, these data suggest that the Δ*trmB* mutant strain has reduced levels of protein glycosylation, which are especially apparent in the S-layer glycoprotein.

The ΔtrmB mutant glycosylation defect is associated with an inadequate supply of carbohydrate precursors

TrmB has been established as a direct positive regulator of gluconeogenic enzyme-coding genes in *H. salinarum* (Schmid *et al.*, 2009; Todor *et al.*, 2013). This transcription factor directly regulates the expression of genes encoding

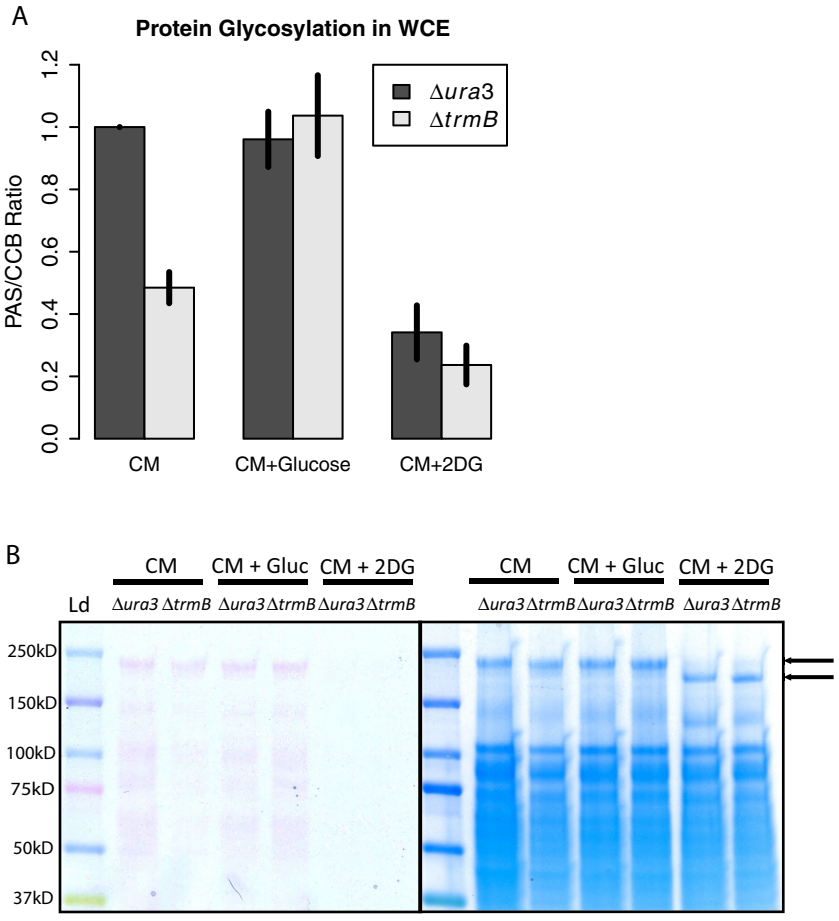

Fig. 2. S-layer protein glycosylation is deficient in the Δ*trmB* mutant strain in the absence of glucose.
A. Bar graph shows the ratio of PAS to CCB intensity in whole cell extracts. In the Δ*ura3* parent strain (dark bars) S-layer protein glycosylation is constant with and without glucose and is inhibited by 2DG. In the Δ*trmB* mutant strain (light bars), glycosylation is impaired in the absence of glucose, and inhibited by 2DG. Error bars represent standard error of an average of 10 replicates.
B. Representative images of PAS stained (left, pink bands) and CCB stained (right, blue bands) SDS-PAGE gels of *H. salinarum* whole cell extracts, showing decreased S-layer and general glycosylation in the Δ*trmB* mutant strain in the absence of glucose and in both strains in the presence of 2DG. The black arrows to the right identify the S-layer band with glycosylation (top arrow) and without (bottom arrow).

enzymes leading from the TCA cycle, through pyruvate, phospho*enol*pyruvate, to fructose 6-phosphate. Since genes encoding gluconeogenic enzymes are expressed at a lower level in the Δ*trmB* mutant than in the Δ*ura3* parent strain in the absence of glucose, we hypothesized that the glycosylation defect observed in the Δ*trmB* mutant strain may be due to reduced supply of glycosylation precursors. However, TrmB regulated gene products are also involved in glycerolipid anabolic pathways. We reasoned that defects in the dolichol phosphate lipid carriers on which the S-layer glycans are built and delivered (Lechner *et al.*, 1985) might also lead to the glycosylation defect of the Δ*trmB* mutant strain. To test this alternative hypothesis, we compared the growth of the mutant and parent strains in CM supplemented with varying amounts of 2DG and the antibiotic bacitracin (Fig. 3A, see Supplementary Table S3 for *P*-values). Bacitracin acts to inhibit glycosylation by preventing dephosphorylation of the dolichol lipid pyrophosphate sugar carrier (Kato *et al.*, 1980), whereas 2DG acts by competing with glucose for incorporation into oligosaccharide chains and terminating these chains upon incorporation in *Saccharomyces cerevisiae* (Johnson, 1968). To confirm that 2DG is a competitive inhibitor of glycosylation in *H. salinarum*, we assayed growth in rich medium supplemented with varying amounts of glucose and 2DG. We found that glucose rescued 2DG toxicity, suggesting that 2DG is a competitive inhibitor (Supplementary Fig. S2). The Δ*trmB* mutant was strikingly more susceptible to 2DG than the parent strain. While the parent strain was able to grow in the presence of up to 3% 2DG, the Δ*trmB* mutant ceased growth in the presence of 1% 2DG (Fig. 3A). Interestingly, we found little difference in the growth inhibitory effect of bacitracin on the Δ*trmB* mutant strain and the isogenic Δ*ura3* parent strain (Fig. 3B, Supplementary Table S3). This observation is consistent with the hypothesis that the Δ*trmB* mutant is inhibited for glycosylation at the level of substrate availability rather than at the level of the lipid carriers involved in delivering sugar moieties to the S-layer. Combined with our previous knowledge that TrmB does not directly regulate the level of S-layer protein or the archaeal glycosylation genes (*agl*), and that genes coding for enzymes involved in gluconeogenesis are downregulated in the Δ*trmB* mutant, these growth data strongly support the hypothesis that the glycosylation defect of the Δ*trmB* mutant strain is caused by a defect in precursor availability.

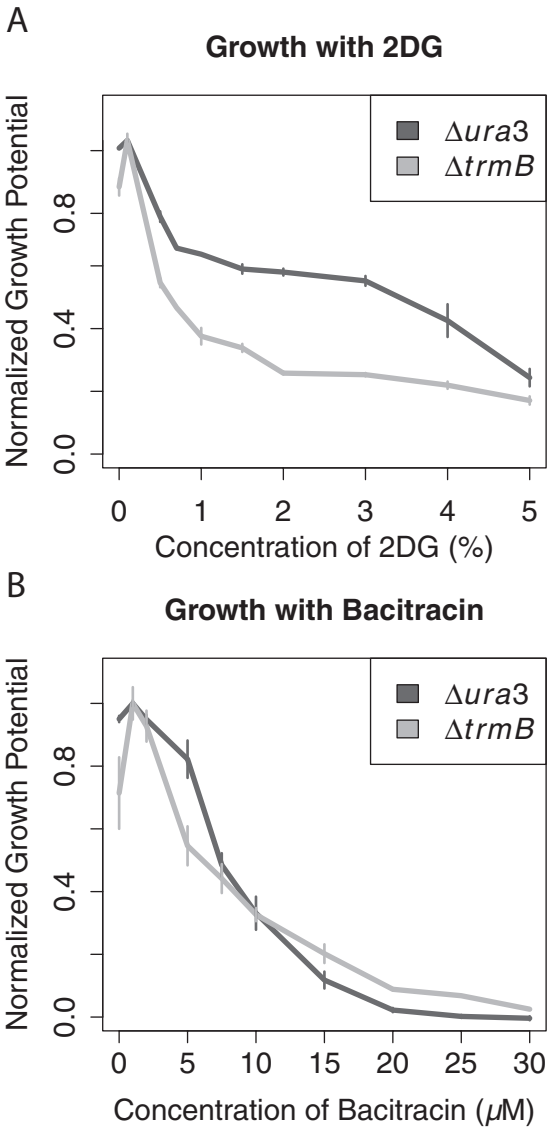

Fig. 3. The Δ*trmB* mutant (light grey line) exhibits impaired growth at lower 2DG (A) concentrations than the Δ*ura3* parent strain (dark grey line). In contrast, the growth inhibition due to bacitracin (B) is constant between the Δ*trmB* mutant (light line) and the Δ*ura3* parent strain (dark line). Growth was measured as the area under the log transformed curve and normalized to the highest growth rate for each strain. Error bars represent standard error of at least two biological replicates, each with at least two technical replicates.

Direct detection of intracellular metabolite concentrations reveals inadequate supply of carbohydrates in the ΔtrmB mutant strain

In order to test whether the Δ*trmB* mutant strain is defective in precursor availability, we measured intracellular metabolites in cell extracts from both strains growing in the presence and absence of glucose. Cells were grown in complete defined medium (CDM) in order to positively ascribe compounds to the organism. We used an untargeted mass spectrometric metabolomics approach (*Experimental procedures*) to identify candidate intermediates, as the specific precursor sugars and their assembly process are not fully characterized for this organism. Several monosaccharides were detected, including aldohexoses and ketohexoses. Sugar levels (relative to all identified metabolites) were significantly lower in the Δ*trmB* mutant compared to those of the Δ*ura3* parent in the absence of glucose (Fig. 4, $P < 6 \times 10^{-3}$), but not in the presence of glucose ($P > 0.8$). The sugar levels in each strain under each condition followed the pattern observed for cell surface carbohydrate staining (Fig. 2) and cell shape (Fig. 1). This suggests that transcriptional regulation of gluconeogenic enzyme-coding genes by TrmB (Schmid *et al.*, 2009) directly affects intracellular metabolite concentrations, which correlate strongly with other Δ*trmB* mutant phenotypes. This is consistent with the hypothesis that an inadequate supply of monosaccharide precursors causes the glycosylation defect in Δ*trmB*.

TrmB activity is correlated with instantaneous growth rate

Our data suggest that TrmB is required for regulating the supply of S-layer glycosylation precursors by controlling gluconeogenesis. Since cell growth and division require additional S-layer production to accommodate the changing cell surface area, and therefore additional glycosylation precursors, we reasoned that TrmB activity could be correlated with instantaneous growth rate. To test this, we reanalysed four expression experiments from the literature (Schmid *et al.*, 2007; Facciotti *et al.*, 2010; Kaur *et al.*, 2010; Beer *et al.*, 2014). Instantaneous growth rate was

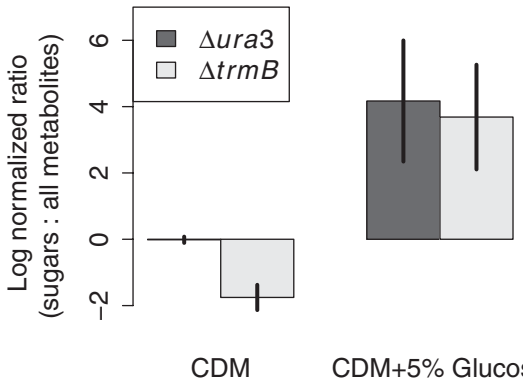

Fig. 4. The Δ*trmB* mutant strain (light bars) is deficient in sugars in the absence of glucose. Glucose complements this phenotype, returning sugar levels to those of the Δ*ura3* isogenic parent strain (dark bars). Each bar represents the log-transformed ratio of summed glucose peak areas versus all identified metabolites normalized to the parent strain grown without glucose. Error bars represent standard error from the mean of three biological replicates.

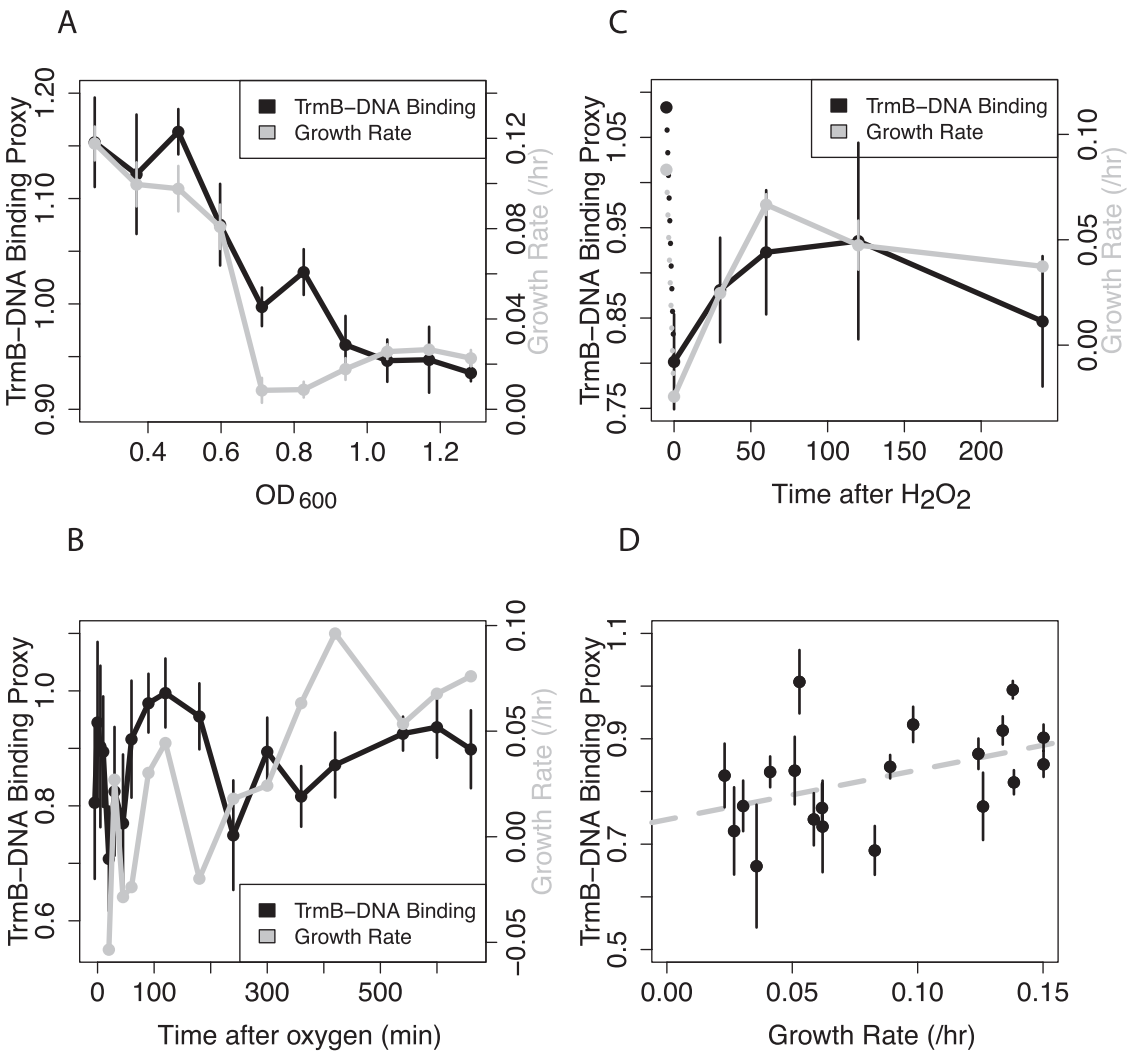

Fig. 5. Inferred TrmB–DNA binding (black line) correlates with growth rate (grey line) across growth in batch culture (A), during the shift from anoxic to oxic conditions in a turbidostat (B), during a sublethal challenge with H_2O_2 (C), and during mid-log phase growth in media of varying salinity (D). The dotted black and grey lines in (C) represent the TrmB–DNA binding and growth rate (respectively) prior to H_2O_2 addition as inferred from the data shown in (A). The dashed grey line in (D) depicts the linear regression between the proxy and growth rate in varying media formulations.

calculated from the optical density of the culture over time. Since TrmB–DNA binding was not measured in these experiments, we derived a gene expression proxy for TrmB binding. To generate this proxy, we calculated a composite average for the expression of genes whose activation (genes encoding enzymes in gluconeogenesis) or repression (genes encoding enzymes in glycolysis) depends exclusively upon TrmB binding (Todor *et al.*, 2013; specific genes listed in *Experimental procedures*). We applied this metric to gene expression data from *H. salinarum* cells (i) throughout the growth curve in batch culture (Facciotti *et al.*, 2010; Fig. 5A), (ii) undergoing the transition from anoxic to oxic physiology (Schmid *et al.*, 2007; Fig. 5B), and (iii) being challenged with a sub-lethal dose of H_2O_2 (Kaur *et al.*, 2010; Fig. 5C). We found that instantaneous growth rate and TrmB activity were significantly and positively correlated across all of these conditions and timescales (Pearson correlation = 0.579, P-value < 10^{-7}). In order to confirm that the correlation between growth rate and TrmB–DNA binding was not due to nutrient changes over time, we reanalysed data from a recent paper (Beer *et al.*, 2014) in which *H. salinarum* was grown in 10 media of varying ion composition but invariant nutrients. All cultures were harvested during balanced growth in mid-log phase (OD_{600} ~ 0.4–0.5). We found that under these conditions, TrmB–DNA binding also correlated significantly with instantaneous growth rate (Pearson correlation = 0.448, P-value < 0.05, Fig. 5D). Together with other data

presented here (Figs 2–4), this proxy is consistent with TrmB linking metabolism with growth rate in order to ensure an appropriate supply of glycosylation precursors under varied environmental conditions.

Discussion

In previous work, we showed that the transcription factor TrmB is important for regulating genes encoding enzymes across the metabolic network of *H. salinarum* (Schmid *et al*., 2009). Specifically, genome-wide expression and TrmB–DNA binding location measurements demonstrated that TrmB regulates the promoters of 113 genes coding for enzymes involved in central carbon metabolism, purine metabolism, cobalamin biosynthesis, and other metabolic processes in response to glucose (Schmid *et al*., 2009). Using dynamic gene expression profiling, we were able to identify the topology of TrmB regulation of central carbon metabolism, purine metabolism, and cobalamin biosynthesis (Todor *et al*., 2013). However, the strong effect of glucose on the many TrmB regulated promoters and the gross morphological (Fig. 1) and growth rate (Schmid *et al*., 2009) defects of the Δ*trmB* mutant strain in the absence of glucose are at odds with observations suggesting that *H. salinarum* cannot metabolize glucose for energy (Gochnauer and Kushner, 1969; Severina *et al*., 1990; Sonawat *et al*., 1990). In order to resolve this discrepancy, we performed a series of focused phenotypic profiling experiments. Combining these data with our previous knowledge of TrmB function, we hypothesize that TrmB is required for proper glycosylation of the S-layer protein by regulating the level of gluconeogenic enzymes that supply monosaccharide precursors from amino acids (Figs 2–4; Schmid *et al*., 2009; Todor *et al*., 2013).

Metabolomics analysis suggests that the concentration of monosaccharides is decreased in the Δ*trmB* mutant in the absence of glucose. Although the assembly pathway for S-layer glycans is not currently known for *H. salinarum*, the low levels of sugars such as hexoses in the Δ*trmB* mutant in the absence of glucose suggest a link between TrmB regulation of gluconeogenesis and S-layer glycoprotein assembly. In *H. salinarum*, TrmB directly regulates the expression of genes coding for gluconeogenic enzymes leading to fructose-6-phosphate, but derivatives of this intermediate other than glucose have not yet been investigated to determine if they complement the Δ*trmB* mutant phenotype. Taken together with the Δ*trmB* mutant's sensitivity to 2DG and its lack of increased sensitivity to bacitracin, these data suggest that TrmB is required for maintaining the level of S-layer glycan precursors, likely by regulating gluconeogenic enzyme-coding genes. Our metabolomics work therefore paves the way for future characterization of glycan synthesis pathways in this organism.

The amount of S-layer protein present in a culture of *H. salinarum* is proportional to the surface area of the cells. Since each S-layer monomer is decorated with specific glycans at specific residues (Wieland, 1988), it follows that the amount of glycosylation is also proportional to the surface area of the cell. Because we did not observe a substantial change in the surface area to volume ratio of cells at different phases of growth (Supplementary Fig. S3), we reasoned that the rate of change in surface area of a culture is proportional to its instantaneous growth rate. Therefore, we propose that the synthesis rate of glycosylation precursors will be proportional to the growth rate of *H. salinarum*. Using a gene expression proxy for TrmB–DNA binding, we found that growth rate is correlated with TrmB–DNA binding activity (Fig. 5). This proxy is a valid metric for TrmB–DNA binding activity because (i) it is well correlated with empirical TrmB–DNA binding measured under other conditions (Schmid *et al*., 2009, Supplementary Fig. S4), (ii) the P*ppsA::GFP* promoter fusion shows an expression pattern across growth consistent with inferred TrmB–DNA binding activity (Supplementary Fig. S5), and (iii) as expected, the proxy reports a constant low level in the Δ*trmB* mutant in the absence and presence of glucose and in the Δ*ura3* parent strain in the presence of glucose (Supplementary Fig. S6). Because TrmB dissociates from the DNA in the presence of glucose, and because the level of TrmB itself appears to be constant throughout growth (Bonneau *et al*., 2007; Schmid *et al*., 2009), changes in TrmB–DNA binding are likely due to changes in intracellular monosaccharide concentration. Because allosteric regulation of gluconeogenic enzymes is weak in many archaea (Fukuda *et al*., 2004; Say and Fuchs, 2010), we hypothesize that higher growth rates deplete the monosaccharide pool as it is used for S-layer glycosylation, thereby increasing TrmB–DNA binding. In contrast, lower growth rates may lead to accumulation of monosaccharides and decrease TrmB–DNA binding. In this way, TrmB could co-ordinate gluconeogenic flux with respect to growth.

The current study provides additional clarity into the evolutionary rationale of TrmB co-regulation of peripheral metabolic pathways such as amino acid metabolism, purine synthesis, and cobalamin synthesis (Schmid *et al*., 2009; Todor *et al*., 2013). Purine and cobalamin demand is influenced both by instantaneous growth rate and by other factors, such as availability in the environment. Because TrmB activity is correlated with growth via the incorporation rate of sugars into the S-layer, TrmB may function as a growth rate-specific regulator for these peripheral pathways as well. Therefore, appropriate expression of these genes encoding enzymes in peripheral pathways requires co-ordinate regulation by TrmB and yet to be determined regulators.

TrmB is widely conserved throughout the archaeal domain, suggesting that it could function as a growth rate responsive regulator in other archaea as well. In the hyperthermophilic archaeon *Pyrococcus furiosus*, a TrmB-like transcription factor, TrmBL1, acts as a global regulator of gluconeogenic and glycolytic genes. Although its physiological inducer is yet to be determined (Lee *et al*., 2008), TrmBL1 appears to function similarly to the Tgr transcription factor of *Thermococcus kodakarensis*. Tgr functions to repress glycolytic genes and to activate gluconeogenic genes in response to glucose (Kanai *et al*., 2007). The Δ*tgr* mutant grows slowly in the absence of glucose, suggesting the potential for a global regulatory role such as the one that had been postulated for *H. salinarum*. Perhaps the most diverged TrmB homologue identified is the MreA protein of the crenarchaeon *Methanosarcina acetivorans* (Reichlen *et al*., 2012). In this organism, MreA controls acetotrophic and methylotrophic pathways in response to an unknown inducer. The Δ*mreA* strain grows slower than the wild-type on acetate due to constitutive downregulation of acetotrophic genes. Although TrmB homologues have been identified and studied in a variety of archaea, TrmB targets and dynamics have only been investigated in *H. salinarum*. Given the wide range of habitats and metabolic activities in the archaeal domain, further study of TrmB homologues and their respective regulons would be fruitful, especially in closely related haloarchaea with different nutrient requirements.

In the most heavily studied representatives of the bacterial and eukaryotic domains, the yeast *S. cerevisiae* and the enterobacteria *E. coli*, the co-ordination of growth rate and metabolism has two components: one dedicated to appropriate carbon flux and one dedicated to appropriate nitrogen flux. In *S. cerevisiae* the sensor and effector system for connecting carbon flux to growth rate is the Ras/cAMP/PKA system, while the primary sensor system for nitrogen flux is the TOR pathway (Ramachandran and Herman, 2011). In *E. coli*, the carbon sensor is Crp, while the nitrogen sensor is Lrp and its downstream effectors (Cho *et al*., 2008; You *et al*., 2013). In *E. coli*, these two systems operate to determine the appropriate proteome partitioning at varied rates of growth and in different environmental conditions (You *et al*., 2013), and the Crp/cAMP system has been shown to respond to nutrients in a growth rate-dependent manner. Given the expansive regulon of TrmB (Schmid *et al*., 2009) as well as its ability to sense nutrient conditions and growth rate, we hypothesize that TrmB plays a role analogous to the Crp and the Ras/cAMP/PKA in *H. salinarum*. Like Crp and the Ras/cAMP/PKA system, TrmB is the primary regulator of some pathways, and a contributing regulator to many others (Schmid *et al*., 2009; Busti *et al*., 2010; Shimada *et al*., 2011; Todor *et al*., 2013). Additionally, mutations in TrmB affect the ability of the cell to make use of certain nutrients and cause a growth defect, similar to mutations in *crp*. Both Crp and the Ras/cAMP/PKA control cell size. Ras/cAMP/PKA has been shown to control mass accumulation (Busti *et al*., 2010), while Crp indirectly controls the accumulation of UDP-Glucose, a metabolite that interacts with FtsZ to determine cell size (Hill *et al*., 2013). Unlike Crp and the Ras/cAMP/PKA system, the direct effector of TrmB in *H. salinarum* remains unknown. While glucose is able to relieve TrmB repression when added to the media, it is not clear whether it is directly interacting with TrmB or whether a second messenger is involved. Regardless, the broad similarities and similar mutant phenotypes of TrmB, Crp, and Ras/cAMP/PKA, suggest that TrmB is acting in an analogous role in *H. salinarum*. Surprisingly, this suggests that despite the lack of protein homology, a conserved transcriptional strategy links growth rate and nutrition across all three domains.

In closing, our findings suggest a transcriptional mechanism for linking cell growth and metabolism in an archaeon. An evolutionarily conserved transcription factor can regulate metabolism by monitoring the anabolic production of a small molecule that is integrated into the cell surface. Interestingly, both TrmB and its *cis*-regulatory motif are well conserved throughout the archaeal domain, suggesting that TrmB could be a conserved mechanism for connecting cell growth and metabolism. The variety of lifestyles and metabolic niches occupied by members of the archaea make TrmB an excellent case study for the co-evolution of transcriptional and metabolic networks in diverse environments. Although much work remains to be done to elucidate the mechanisms of co-ordinated control of cell shape, cell cycle, and growth rate in archaea, our findings represent a first step in understanding how archaea sense and respond to changes in cell growth in their extreme and varied environments. Combined with previous research on the TrmB responsive gene regulatory network, this work paves the way for future studies on the conservation of the topology underlying this connection across all three domains.

Experimental procedures

Strains and plasmids

Halobacterium salinarum NRC-1 (ATCC strain 700922) was used as the wild-type strain background. Experiments were performed in previously constructed strains, one containing an in-frame deletion of *VNG1451C* (Δ*ura3*Δ*trmB*; Schmid *et al*., 2009) and its isogenic parent strain, Δ*ura*3 (Peck *et al*., 2000).

Growth conditions

Cells were grown in either Complete Defined Medium (CDM) containing 19 amino acids (Todor *et al*., 2013) or rich

complete medium (CM; 250 NaCl, 20 g l^{-1} $MgSO_4$ $7H_2O$, 3 g l^{-1} sodium citrate, 2 g l^{-1} KCl, 10 g l^{-1} bacteriological peptone) as indicated in the figures. Each medium formulation was supplemented with 50 μg ml^{-1} uracil to complement the *ura3* deletion. Cultures were routinely grown at 42°C with shaking at 225 r.p.m. under low ambient light. In order to assess growth under different conditions, 200 μl cultures were grown at 42°C under continuous shaking (~ 225 r.p.m.) in a Bioscreen C automated growth curve analysis system (Growth Curves USA, Piscataway, NJ). Optical density at 600 nm was measured every 30 min for up to 200 culture samples simultaneously. Maximum instantaneous growth rate was calculated from the log transformed and LOWESS smoothed data. Area under the log transformed growth curve (growth potential) was used as an additional growth metric to convey information about both growth rate and carrying capacity of the culture. These calculations are packaged into the bsd Analysis Function freely available at http://gaggle.systemsbiology.net/svn/gaggle/BioscreenUtilsR/trunk/bsdAnalysisFunc.R.

Cell lysis, S-layer enrichment, and staining protocol

S-layer glycosylation levels were quantified in whole cell extracts and in S-layer enrichments from each of the *Δura3* and *ΔtrmB* strains. For preparation of whole cell extracts, *H. salinarum* cultures were grown to stationary phase (OD_{600} ~ 1) in CM medium with or without glucose. Equivalent cell numbers from each strain were pelleted by centrifugation at 21 130 r.c.f. for 30 s and lysed in 500 μl of water followed by vigorous pipetting to lyse and homogenize the samples. Several aliquots of different volumes (50, 100, 200 μl) were precipitated using trichloroacetic acid and separated by SDS-PAGE as described below. S-layer enrichment was performed using a modified version of the protocol described in Sumper *et al.* (1990). Briefly, *H. salinarum* cultures were grown to mid-log phase (OD_{600} ~ 0.6) in CM medium with or without glucose. Approximately 10 ml of culture was pelleted at 4500 r.c.f. for 10 min, resuspended in basal salts buffer (BS; CM lacking peptone) containing EDTA equimolar to the Mg^{2+} concentration (80 mM), and incubated for 30 min at 225 r.p.m. at 42°C to remove the S-layer. Cells were removed by centrifugation for 5 min at 12 000 r.c.f. The supernatant, which contains primarily S-layer protein, was collected. Proteins were precipitated using 10% TCA, solubilized in Laemmli buffer containing SDS, and separated on two identically loaded Bio-Rad Mini Protean TGX gels for 1 h at 125V (Bio-Rad Laboratories, Hercules, CA). One gel was stained to visualize protein using Colloidal Coomassie Blue (CCB; Invitrogen, Carlsbad, CA), and the other was stained to visualize carbohydrate using Periodic Acid Schiff (PAS; Sigma, St. Louis, MO). After staining, gels were scanned using an Epson Perfection V700 Photo scanner and the band corresponding to the S-layer glycoprotein, known to run at ~ 200 kD (Lechner and Wieland, 1989), was quantified on each stained gel using ImageJ software. The PAS/CCB ratio for each of *Δura3* and *ΔtrmB* with and without glucose was normalized to the average ratio of *Δura*3 without glucose for every gel, and the results from at least two bands were averaged to calculate the final values.

Microscopy and image quantification

Cells were mounted on agarose pads and imaged using a Zeiss Axio Scope.A1 (Carl Zeiss, Oberkochen, Germany) and a PixelLINK CCD (PixelLINK, Ottawa, Canada) camera. Images were captured using a 100× oil immersion objective under phase-contrast illumination. Image analysis was performed in ImageJ. Briefly, each image was automatically thresholded using the IsoData iterative thresholding scheme (Velasco, 1980). Ellipses were fit to all shapes with circularity (minor/major axis) between 0.1 and 1 and area between 300 and 3000 pixels (equivalent to 0.78 $μM^2$–7.8 $μM^2$). The major and minor axes were used as the cell length and width respectively. Significance of differences between the ratio of length/width of *ΔtrmB* versus *Δura3* was calculated using the two-tailed Welch's *t*-test. This test and Bonferroni correction for multiple hypothesis testing are used where relevant for comparisons reported throughout the study (see also Supplementary Tables S1–S3).

Collection and analysis of GC-MS samples

Biological triplicate cultures of Δ*ura3* parent and Δ*trmB* mutant strains were grown to mid-logarithmic phase (OD_{600} ~ 0.3–0.6) in CDM with or without the addition of 5% glucose as described above. Each sample was pelleted by centrifugation for 10 min at 4500 r.c.f., washed twice with BS buffer, lysed in 0.2% of culture volume of sterile H_2O, and centrifuged at 18 000 r.c.f. for 5 min to remove cellular debris. Five volumes of methanol were added to each lysate to precipitate macromolecules. The extracts were mixed and centrifuged again at 18 000 r.c.f. for 5 min. The methanolic supernatant was transferred to a clean tube and 5 μl of 2.5 mg ml^{-1} myristic acid-D27 (Sigma-Aldrich, St. Louis, MO) was added as an internal standard. Samples were then dried under forced nitrogen at 45°C. Spin-vacuum and azeotropic treatment under ethyl acetate were applied to allow complete drying of high-salt samples. Dried samples were derivatized by stepwise addition of (i) 100 μl of 20 mg ml^{-1} methoxyamine hydrochloride in pyridine (Sigma-Aldrich), and (ii) 300 μl MSTFA with 1% TMCS (Thermo Fisher Scientific, Waltham, WA) with 50°C incubations (stagnant) for 30 min following addition of each chemical. After derivatization, samples were cooled, mixed, pulse centrifuged, and the liquid phase was transferred to GC/MS vials. Non-targeted metabolomics via GC/MS and peak area calculation were performed as described in Scholtens *et al.* (2014). Raw peak areas (unlogged values) for all sugars were summed independently for each strain, condition and biological replicate. Each of these sums were divided by the sum of all identified metabolites from the same sample and normalized to the mean ratio for the parent strain grown without glucose. The log transformed mean across biological replicates of these normalized values are reported in Fig. 4.

Analysis of microarray and growth data

To infer TrmB–DNA binding activity across a range of conditions, we adapted the concept of a gene expression proxy from work in *S. cerevisiae* (Airoldi *et al.*, 2009). The proxy was defined as the average of gene expression of *VNG0095G,*

VNG0330G, VNG0683C, VNG0684G, VNG1216G, VNG1887G (TrmB-activated genes coding for enzymes in the hypothesized gluconeogenic pathway) and the reciprocal of *VNG0324G* and *VNG0937G* (TrmB-repressed genes coding for enzymes that catalyse the reverse reaction of *VNG0330G* and *VNG0095G* respectively). Gene expression values were obtained from published microarray data for *H. salinarum* throughout growth in batch culture (Facciotti *et al*., 2010; GEO Accession No. GSE14832, GSE14835 and GSE14836), from *H. salinarum* undergoing the transition from anaerobic to aerobic conditions (Schmid *et al*., 2007; GEO Accession No. GSE7559), from *H. salinarum* being exposed to H_2O_2 (Kaur *et al*., 2010; GEO Accession No. GSE17515), and from *H. salinarum* growing in media of different salinity (Beer *et al*., 2014; GEO Accession No. GSE53544). Growth rate at each time point was calculated as the weighted average of the growth rate before and after each time point. The first four points of the oxygen time-course were excluded due to optical density changes caused by the foaming of the medium during sparging of oxygen (Schmid *et al*., 2007). The batch culture growth data were binned according to optical density range. Figure 5A shows the bin averages and standard error of eight independent time-course experiments comprising 56 separate microarrays.

Acknowledgements

This material is based upon work supported by the National Science Foundation under Grant numbers MCB-1052290 and MCB-1417750 to AKS. We would like to acknowledge Lee Pang for conceptualizing and creating the bsdAnalysis function and for refining it to work seamlessly with Bioscreen files. We thank Karlyn Beer for supplying growth data from media of different salinities. The authors have no conflicts of interest to report.

References

Abu-Qarn, M., Yurist-Doutsch, S., Giordano, A., Trauner, A., Morris, H.R., Hitchen, P., *et al*. (2007) *Haloferax volcanii* AglB and AglD are involved in N-glycosylation of the S-layer glycoprotein and proper assembly of the surface layer. *J Mol Biol* **374:** 1224–1236.

Airoldi, E.M., Huttenhower, C., Gresham, D., Lu, C., Caudy, A.A., Dunham, M.J., *et al*. (2009) Predicting cellular growth from gene expression signatures. *PLoS Comput Biol* **5:** e1000257.

Beer, K.D., Wurtmann, E.J., Pinel, N., and Baliga, N.S. (2014) Model organisms retain an 'ecological memory' of complex ecologically relevant environmental variation. *Appl Environ Microbiol* **80:** 1821–1831.

Bonneau, R., Facciotti, M.T., Reiss, D.J., Schmid, A.K., Pan, M., Kaur, A., *et al*. (2007) A predictive model for transcriptional control of physiology in a free living cell. *Cell* **131:** 1354–1365.

Brauer, M.J., Huttenhower, C., Airoldi, E.M., Rosenstein, R., Matese, J.C., Gresham, D., *et al*. (2008) Coordination of growth rate, cell cycle, stress response, and metabolic activity in yeast. *Mol Biol Cell* **19:** 352–367.

Busti, S., Coccetti, P., Alberghina, L., and Vanoni, M. (2010) Glucose signaling-mediated coordination of cell growth and cell cycle in *Saccharomyces cerevisiae*. *Sensors (Basel)* **10:** 6195–6240.

Cho, B.K., Barrett, C.L., Knight, E.M., Park, Y.S., and Palsson, B.O. (2008) Genome-scale reconstruction of the Lrp regulatory network in *Escherichia coli*. *Proc Natl Acad Sci USA* **105:** 19462–19467.

Esko, J.D., and Bertozzi, C. (2009) Chemical tools for inhibiting glycosylation. In *Essentials of Glycobiology*, 2nd edn. Varki, A., Cummings, R.D., Esko, J.D., Freeze, H., Stanley, P., Bertozzi, C., *et al*. (eds). Cold Spring Harbor, NY: Cold Spring Harbor Laboratory Press, Chapter 50.

Facciotti, M.T., Pang, W.L., Lo, F.Y., Whitehead, K., Koide, T., Masumura, K., *et al*. (2010) Large scale physiological readjustment during growth enables rapid, comprehensive and inexpensive systems analysis. *BMC Syst Biol* **4:** 64.

Fukuda, W., Fukui, T., Atomi, H., and Imanaka, T. (2004) First characterization of an archaeal GTP-dependent phosphoenolpyruvate carboxykinase from the hyperthermophilic archaeon *Thermococcus kodakaraensis* KOD1. *J Bacteriol* **186:** 4620–4627.

Gochnauer, M.B., and Kushner, D.J. (1969) Growth and nutrition of extremely halophilic bacteria. *Can J Microbiol* **15:** 1157–1165.

Gralnick, H.R., Jackson, G.M., Williams, S.B., and Cregger, M.C. (1982) Factor VIII/von Willebrand factor protein: sensitivity of periodic acid Schiff stain to carbohydrate deficiency. *Blood* **59:** 1310–1316.

Herrmann, U., and Soppa, J. (2002) Cell cycle-dependent expression of an essential SMC-like protein and dynamic chromosome localization in the archaeon *Halobacterium salinarum*. *Mol Microbiol* **46:** 395–409.

Hill, N.S., Buske, P.J., Shi, Y., and Levin, P.A. (2013) A moonlighting enzyme links *Escherichia coli* cell size with central metabolism. *PLoS Genet* **9:** e1003663.

Johnson, B.F. (1968) Lysis of yeast cell walls induced by 2-deoxyglucose at their sites of glucan synthesis. *J Bacteriol* **95:** 1169–1172.

Johnston, G.C., Pringle, J.R., and Hartwell, L.H. (1977) Coordination of growth with cell division in the yeast *Saccharomyces cerevisiae*. *Exp Cell Res* **105:** 79–98.

Kanai, T., Akerboom, J., Takedomi, S., van de Werken, H.J., Blombach, F., van der Oost, J., *et al*. (2007) A global transcriptional regulator in *Thermococcus kodakaraensis* controls the expression levels of both glycolytic and gluconeogenic enzyme-encoding genes. *J Biol Chem* **282:** 33659–33670.

Kato, S., Tsuji, M., Nakanishi, Y., and Suzuki, S. (1980) Enzymatic dephosphorylation of dolichyl pyrophosphate – the bacitracin-sensitive, rate-limiting step for dolichyl mannosyl phosphate synthesis in rat liver microsomes. *Biochem Biophys Res Commun* **95:** 770–776.

Kaur, A., Van, P.T., Busch, C.R., Robinson, C.K., Pan, M., Pang, W.L., *et al*. (2010) Coordination of frontline defense mechanisms under severe oxidative stress. *Mol Syst Biol* **6:** 393.

Krug, M., Lee, S.J., Diederichs, K., Boos, W., and Welte, W. (2006) Crystal structure of the sugar binding domain of the archaeal transcriptional regulator TrmB. *J Biol Chem* **281:** 10976–10982.

Lechner, J., and Wieland, F. (1989) Structure and biosynthe-

sis of prokaryotic glycoproteins. *Annu Rev Biochem* **58:** 173–194.
Lechner, J., Wieland, F., and Sumper, M. (1985) Transient methylation of dolichyl oligosaccharides is an obligatory step in halobacterial sulfated glycoprotein biosynthesis. *J Biol Chem* **260:** 8984–8989.
Lee, S.J., Engelmann, A., Horlacher, R., Qu, Q., Vierke, G., Hebbeln, C., *et al*. (2003) TrmB, a sugar-specific transcriptional regulator of the trehalose/maltose ABC transporter from the hyperthermophilic archaeon *Thermococcus litoralis*. *J Biol Chem* **278:** 983–990.
Lee, S.J., Surma, M., Seitz, S., Hausner, W., Thomm, M., and Boos, W. (2007) Characterization of the TrmB-like protein, PF0124, a TGM-recognizing global transcriptional regulator of the hyperthermophilic archaeon *Pyrococcus furiosus*. *Mol Microbiol* **65:** 305–318.
Lee, S.J., Surma, M., Hausner, W., Thomm, M., and Boos, W. (2008) The role of TrmB and TrmB-like transcriptional regulators for sugar transport and metabolism in the hyperthermophilic archaeon *Pyrococcus furiosus*. *Arch Microbiol* **190:** 247–256.
Mescher, M.F., and Strominger, J.L. (1976) Structural (shape-maintaining) role of the cell surface glycoprotein of *Halobacterium salinarium*. *Proc Natl Acad Sci USA* **73:** 2687–2691.
Mescher, M.F., Strominger, J.L., and Watson, S.W. (1974) Protein and carbohydrate composition of the cell envelope of *Halobacterium salinarium*. *J Bacteriol* **120:** 945–954.
Ng, W.V., Kennedy, S.P., Mahairas, G.G., Berquist, B., Pan, M., Shukla, H.D., *et al*. (2000) Genome sequence of *Halobacterium* species NRC-1. *Proc Natl Acad Sci USA* **97:** 12176–12181.
Peck, R.F., Dassarma, S., and Krebs, M.P. (2000) Homologous gene knockout in the archaeon *Halobacterium salinarum* with *ura3* as a counterselectable marker. *Mol Microbiol* **35:** 667–676.
Perez-Rueda, E., and Janga, S.C. (2010) Identification and genomic analysis of transcription factors in archaeal genomes exemplifies their functional architecture and evolutionary origin. *Mol Biol Evol* **27:** 1449–1459.
Ramachandran, V., and Herman, P.K. (2011) Antagonistic interactions between the cAMP-dependent protein kinase and Tor signaling pathways modulate cell growth in *Saccharomyces cerevisiae*. *Genetics* **187:** 441–454.
Reichlen, M.J., Vepachedu, V.R., Murakami, K.S., and Ferry, J.G. (2012) MreA functions in the global regulation of methanogenic pathways in *Methanosarcina acetivorans*. *MBio* **3:** e00189-00112.
Say, R.F., and Fuchs, G. (2010) Fructose 1,6-bisphosphate aldolase/phosphatase may be an ancestral gluconeogenic enzyme. *Nature* **464:** 1077–1081.
Schmid, A.K., Reiss, D.J., Kaur, A., Pan, M., King, N., Van, P.T., *et al*. (2007) The anatomy of microbial cell state transitions in response to oxygen. *Genome Res* **17:** 1399–1413.
Schmid, A.K., Reiss, D.J., Pan, M., Koide, T., and Baliga, N.S. (2009) A single transcription factor regulates evolutionarily diverse but functionally linked metabolic pathways in response to nutrient availability. *Mol Syst Biol* **5:** 282.
Scholtens, D.M., Muehlbauer, M.J., Daya, N.R., Stevens, R.D., Dyer, A.R., Lowe, L.P., *et al*. (2014) Metabolomics reveals broad-scale metabolic perturbations in hyperglycemic mothers during pregnancy. *Diabetes Care* **37:** 158–166.
Severina, L.O., Pimenov, N.V., and Plakunov, V.K. (1990) Glucose transport into the extremely halophilic archaebacteria. *Arch Microbiol* **155:** 131–136.
Shimada, T., Fujita, N., Yamamoto, K., and Ishihama, A. (2011) Novel roles of cAMP receptor protein (CRP) in regulation of transport and metabolism of carbon sources. *PLoS ONE* **6:** e20081.
Sonawat, H.M., Srivastava, S., Swaminathan, S., and Govil, G. (1990) Glycolysis and Entner-Doudoroff pathways in *Halobacterium halobium*: some new observations based on 13C NMR spectroscopy. *Biochem Biophys Res Commun* **173:** 358–362.
Sumper, M., Berg, E., Mengele, R., and Strobel, I. (1990) Primary structure and glycosylation of the S-layer protein of *Haloferax volcanii*. *J Bacteriol* **172:** 7111–7118.
Todor, H., Sharma, K., Pittman, A.M., and Schmid, A.K. (2013) Protein–DNA binding dynamics predict transcriptional response to nutrients in archaea. *Nucleic Acids Res* **41:** 8546–8558.
Van, P.T., Schmid, A.K., King, N.L., Kaur, A., Pan, M., Whitehead, K., *et al*. (2008) *Halobacterium salinarum* NRC-1 PeptideAtlas: toward strategies for targeted proteomics and improved proteome coverage. *J Proteome Res* **7:** 3755–3764.
Velasco, F.R. (1980) Thresholding using the ISODATA clustering algorithm. *IEEE Trans Syst Man Cybern* **10:** 771–774.
Weart, R.B., Lee, A.H., Chien, A.C., Haeusser, D.P., Hill, N.S., and Levin, P.A. (2007) A metabolic sensor governing cell size in bacteria. *Cell* **130:** 335–347.
Wieland, F. (1988) Structure and biosynthesis of prokaryotic glycoproteins. *Biochimie* **70:** 1493–1504.
You, C., Okano, H., Hui, S., Zhang, Z., Kim, M., Gunderson, C.W., *et al*. (2013) Coordination of bacterial proteome with metabolism by cyclic AMP signalling. *Nature* **500:** 301–306.

Supporting information

Additional supporting information may be found in the online version of this article at the publisher's web-site.